

A Simple Algorithm for Higher-order Delaunay Mosaics and Alpha Shapes

Herbert Edelsbrunner 

IST Austria (Institute of Science and Technology Austria), Am Campus 1,
3400 Klosterneuburg, Austria
edels@ist.ac.at

Georg Osang* 

IST Austria (Institute of Science and Technology Austria), Am Campus 1,
3400 Klosterneuburg, Austria
georg.osang@ist.ac.at*

1 — Abstract

2 We present a simple algorithm for computing higher-order Delaunay mosaics that works in Euclidean
3 spaces of any finite dimensions. The algorithm selects the vertices of the order- k mosaic from
4 incrementally constructed lower-order mosaics and uses an algorithm for weighted first-order Delaunay
5 mosaics as a black-box to construct the order- k mosaic from its vertices. Beyond this black-box, the
6 algorithm uses only combinatorial operations, thus facilitating easy implementation. We extend this
7 algorithm to compute higher-order α -shapes and provide open-source implementations. We present
8 experimental results for properties of higher-order Delaunay mosaics of random point sets.

2012 ACM Subject Classification Mathematics of computing → Combinatorial algorithms

Keywords and phrases Delaunay mosaics, Voronoi tessellations, algorithms, software, computational experiments.

Funding This project has received funding from the European Research Council (ERC) under the European Union's Horizon 2020 research and innovation programme, grant no. 788183, from the Wittgenstein Prize, Austrian Science Fund (FWF), grant no. Z 342-N31, and from the DFG Collaborative Research Center TRR 109, 'Discretization in Geometry and Dynamics', Austrian Science Fund (FWF), grant no. I 02979-N35.

Lines 489



© Herbert Edelsbrunner and Georg Osang;
licensed under Creative Commons License CC-BY
Leibniz International Proceedings in Informatics

LIPICs Schloss Dagstuhl – Leibniz-Zentrum für Informatik, Dagstuhl Publishing, Germany

1 Introduction

Order- k Voronoi tessellations are a generalization of ordinary Voronoi tessellations. Instead of each domain corresponding to a single point in the input, $A \subseteq \mathbb{R}^d$, each order- k domain corresponds to a subset, $Q \subseteq A$, of size k , and consists of the set of points $x \in \mathbb{R}^d$ for whom the points in Q are the closest k points within A . Its dual is the order- k Delaunay mosaic. We will formally define both in Section 2. Order- k Voronoi tessellations were introduced by [21] as a data structure for fast k closest point queries, namely in time $O(k + \log n)$ with $n = \#A$. A less direct application is the computation of the distance-to-measure introduced in [5] and related to k closest point search in [13]. Furthermore, certain subcomplexes of the order- k Delaunay mosaic realize the order- k α -shapes introduced in [14]. Order- k α -shapes are a generalization of α -shapes [9] used to approximate the shape of a point set. Unlike ordinary α -shapes and depending on the parameter k , they exhibit robustness to noisy data points.

In the plane, the number of domains in the order- k Voronoi tessellation or, equivalently, the number of vertices in the order- k Delaunay mosaic is $\Theta(k(n - k))$; see [15, 21]. For dimensions $d \geq 3$, this number can vary significantly depending on the way the input points are distributed. The upper bound of $O(k^{\lceil \frac{d+1}{2} \rceil} n^{\lfloor \frac{d+1}{2} \rfloor})$ on the total size of the first k higher-order Delaunay mosaics [6] is tight, while the lower bound of $\Omega(k^d n)$ [17] is only conjectured. For individual order- k Delaunay mosaics, the complexity is poorly understood. The problem is closely related to the $(d + 1)$ -dimensional k -set problem. Specifically, the points in $A \subseteq \mathbb{R}^d$ can be mapped to equally many points in \mathbb{R}^{d+1} such that the order- k domains in \mathbb{R}^d correspond to k -sets in \mathbb{R}^{d+1} , see e.g. [6].

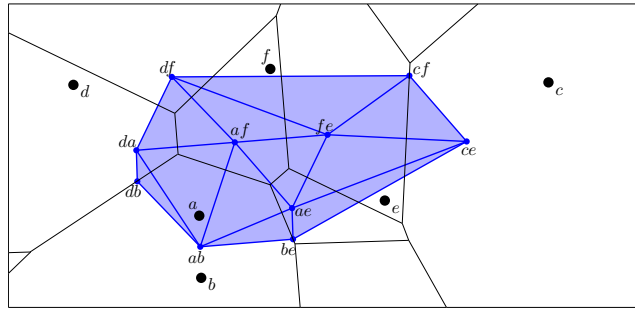
The first algorithm to compute order- k Voronoi tessellations and Delaunay mosaics in the plane was described by Lee in [15]. The algorithm computes the Voronoi tessellations one by one, in increasing order and in time $O(k^2 n \log n)$. Mulmuley [17] extended this algorithm beyond two dimensions, computing the first k levels in a special $(d + 1)$ -dimensional hyperplane arrangement, which implicitly yield the order- k Voronoi tessellations and Delaunay mosaics in time $O(s \log n + k^d n^2)$, in which s denotes the output size. Mulmuley [18] later described another algorithm, which instead adds hyperplanes one by one, and runs in time $O(k^{\lceil \frac{d+1}{2} \rceil} n^{\lfloor \frac{d+1}{2} \rfloor})$ for $d \geq 3$, which equals the worst-case output size. For $d = 2$, the expected runtime is $O(k^2 n \log \frac{n}{k})$. Another incremental algorithm with similar complexity for $d \geq 3$ has been described by Agarwal *et al.* [1].

In this paper, we describe a new algorithm for computing order- k Delaunay mosaics in Euclidean space of any finite dimension that stands out in its simplicity. It employs an algorithm for weighted first-order Delaunay mosaics, and otherwise uses only combinatorial operations. It thus benefits from highly optimized existing implementations and, if desired, can build upon their use of exact arithmetic. Its complexity depends on the complexity of the algorithm used for weighted Delaunay mosaics. Assuming it is linear in its output size, then our algorithm is also linear in its output size. We implement this algorithm and run it on various point sets, shedding light on the size and other properties of order- k Delaunay mosaics. In particular, we compare the total size of the first k Delaunay mosaics of random point sets with the (tight) worst-case upper bound, and we study the size of individual order- k Delaunay mosaics, for which no tight bounds are known in general. As far as we are aware, no such experimental investigations have been performed in the past, possibly due to the lack of a practical algorithm. We extend our algorithm to compute the radius function on an order- k Delaunay mosaic, which gives us the subcomplexes realizing order- k α -shapes. Open-source implementations of our algorithm are available [19, 20].

56 Our algorithm makes use of the *rhomboid tiling* [10], which we will introduce in Section 2
 57 alongside other necessary definitions. We will explore the combinatorial properties of this
 58 tiling and, by proxy, the properties of order- k Delaunay mosaics in Section 3. Using these
 59 results, we explain our algorithm in Section 4. We present experimental results obtained with
 60 two implementations of this algorithm in Section 5. Section 6 introduces a radius function
 61 on the order- k Delaunay mosaics and a way to compute it to yield order- k α -shapes. We
 62 close with a discussion of possible extensions and optimizations in Section 7.

63 2 Definitions

67 Given a locally finite set, $A \subseteq \mathbb{R}^d$, the (*Voronoi*) *domain* of $Q \subseteq A$ is $\text{dom}(Q) = \{x \in$
 68 $\mathbb{R}^d \mid \|x - q\| \leq \|x - a\|, \forall q \in Q, \forall a \in A \setminus Q\}$. Its *order* is $\#Q$. For each positive integer k ,
 69 the *order- k Voronoi tessellation* is $\text{Vor}_k(A) = \{\text{dom}(Q) \mid Q \subseteq A, \#Q = k\}$. The *order- k*
 70 *Delaunay mosaic* is the cell complex dual to $\text{Vor}_k(A)$, denoted $\text{Del}_k(A)$. To realize the
 71 mosaic geometrically, we usually use the average of the points in Q as the location of the
 72 corresponding vertex in \mathbb{R}^d . In a few instances we use the sum rather than the average,
 73 for convenience. Figure 1 shows an example for $k = 2$. As we will see shortly, in $d \geq 3$
 74 dimensions, the order- k Delaunay mosaic is not necessarily simplicial even if the points are
 in general position.



64 ■ **Figure 1** Superposition of the order-2 Voronoi tessellation (in *black*) and the order-2 Delaunay
 65 mosaic (in *blue*) of a set of six points in the plane. Each domain of the tessellation corresponds to
 66 two of these six points, and the corresponding vertex of the mosaic is the average of these two points.

75
 76 Assuming A is in general position, [10] established the existence of a tiling in \mathbb{R}^{d+1} whose
 77 horizontal integer slices are the Delaunay mosaics. We recall the definition of the tiling and
 78 its most important properties. Let $A \subseteq \mathbb{R}^d$ be locally finite and in general position. We
 79 construct a rhomboid, ϱ , for each partition $A = A_{in} \sqcup A_{on} \sqcup A_{out}$ for which there exists a
 80 sphere S in \mathbb{R}^d such that all points in A_{in} lie inside S , all points in A_{on} lie on S , and all
 81 points in A_{out} lie outside S . Whenever convenient, we write $A_{in}(\varrho) = A_{in}$, $A_{on}(\varrho) = A_{on}$,
 82 and $A_{out}(\varrho) = A_{out}$ to indicate the correspondence. Due to general position of A , we have
 83 $\#A_{on} \leq d + 1$. A *combinatorial vertex* of ϱ is a collection of points that contains A_{in} and is
 84 contained in $A_{in} \cup A_{on}$, and we write

$$85 \quad V(\varrho) = \{A_{in} \subseteq Q \subseteq A_{in} \cup A_{on}\} \tag{1}$$

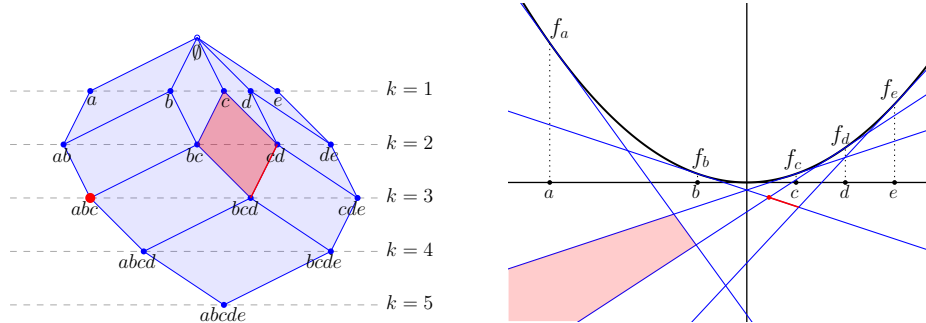
86 for the collection of combinatorial vertices of ϱ . Setting $y_a = (a, -1) \in \mathbb{R}^{d+1}$, for every $a \in A$,
 87 we draw the rhomboids in \mathbb{R}^{d+1} by mapping every combinatorial vertex to $y_Q = \sum_{q \in Q} y_q$, in
 88 which $y_\emptyset = 0$, by convention. The $(d + 1)$ -st coordinate of y_Q is therefore $-\#Q$, and we call
 89 $\#Q$ the *depth* of the vertex. The geometric realization of a rhomboid ϱ is the convex hull of

90 the locations of its combinatorial vertices, which is a rhomboid. We refer to $A_{in}(\varrho)$ as the
 91 *anchor vertex* of ϱ .

92 The *rhomboid tiling* of A , denoted $\text{Rho}(A)$, is the collection of thus defined rhomboids.
 93 By assumption of general position, every face of a rhomboid is again defined by a sphere
 94 as described above and thus belongs to the rhomboid tiling. As proved in [10], any two
 95 rhomboids are either disjoint or intersect in a common face, which implies that the rhomboid
 96 tiling is a complex embedded in \mathbb{R}^{d+1} ; see Figure 2 for an example. The following properties
 97 have been observed in [10]:

- 98 ► **Proposition 1 (Rhomboid Tiling).** *Let $A \subseteq \mathbb{R}^d$ be locally finite and in general position.*
 99 1. $\text{Rho}(A)$ is dual to an arrangement of hyperplanes in \mathbb{R}^{d+1} ;
 100 2. the slice of $\text{Rho}(A)$ at depth k is the order- k Delaunay mosaic of A , scaled by a factor k .

110 The hyperplane arrangement will be introduced in Section 3.2. We elaborate on the second
 111 property: that each cell of the order- k Delaunay mosaic is a slice of some rhomboid. Com-
 112 binatorially, each rhomboid is a cube and, again combinatorially, each cell of $\text{Del}_k(A)$ is a
 113 slice orthogonal to the cube diagonal that passes through a non-empty set of the vertices.
 114 For the $(d + 1)$ -cube, there are $d + 2$ such slices, which we index from top to bottom by
 115 the *generation* $0 \leq g \leq d + 1$. The g -th slice passes through $\binom{d+1}{g}$ vertices, so we have
 116 a vertex at generations $g = 0, d + 1$, a d -simplex at generations $g = 1, d$, and some other
 117 d -dimensional polytope at generations $2 \leq g \leq d - 1$. In $d + 1 = 3$ dimensions, we have a
 118 vertex, a triangle, another triangle, and another vertex, see Figure 4; but already in $d + 1 = 4$
 119 dimensions, the middle slice is not a simplex; see Figure 3. We remark that in addition to
 120 the order- k Delaunay mosaic, also the degree- k Delaunay mosaic, which is the dual of the
 degree- k Voronoi tessellation [11], can be obtained as a slice of $\text{Rho}(A)$ at depth $k - \frac{1}{2}$.

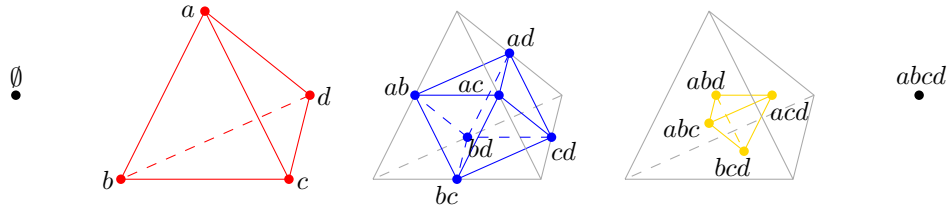


101 ■ **Figure 2** Left: the rhomboid tiling of five points in \mathbb{R}^1 . The highlighted rhomboid defined by
 102 $A_{in} = \{c\}$ and $A_{on} = \{b, d\}$ is the convex hull of the points $y_c, y_{\{b,c\}}, y_{\{c,d\}},$ and $y_{\{b,c,d\}}$. The
 103 horizontal line at depth k intersects the tiling in the order- k Delaunay mosaic. Right: the dual
 104 hyperplane arrangement. Following the dotted lines connecting the points of A on the horizontal
 105 axis to the paraboloid, we find the corresponding tangent hyperplanes. The highlighted rhomboids
 106 of dimension $j = 0, 1, 2$ are dual to the highlighted cells of dimension $2 - j$ in the arrangement.

121

122 3 Combinatorial Properties

123 As proved in [4], the order- k Delaunay mosaic is the projection of the boundary complex
 124 of a convex polyhedron in \mathbb{R}^{d+1} . To explain this construction, we define the *lift* of $a \in \mathbb{R}^d$
 125 as the point $\text{lift}(a) = (a, \|a\|^2) \in \mathbb{R}^{d+1}$. For each k -tuple $Q \subseteq A$, we take the barycenter of
 126 their lifts, $\frac{1}{k} \sum_{q \in Q} \text{lift}(q)$, and obtain the order- k Delaunay mosaic as the vertical projection



107 ■ **Figure 3** Slices of a 4-dimensional rhomboid defined by $A_{in}(\varrho) = \emptyset$ and $A_{on}(\varrho) = \{a, b, c, d\}$. The
 108 non-trivial slices are a tetrahedron at generation $g = 1$, an octahedron at generation $g = 2$, and
 109 another tetrahedron at generation $g = 3$.

127 of the lower faces of the convex hull of these barycenters. Equivalently, we can interpret
 128 each barycenter of lifts as a weighted point in \mathbb{R}^d and get the order- k Delaunay mosaic as
 129 the weighted order-1 Delaunay mosaic of the weighted points. By itself, this approach does
 130 not scale well with k since there are $\binom{\#A}{k}$ such barycenters. Most barycenters, however,
 131 are irrelevant as they do not contribute to the lower faces of the convex hull. If we could,
 132 somehow, identify the relevant barycenters without wasting time on the irrelevant ones, this
 133 procedure would efficiently construct the cells of the order- k Delaunay mosaic by computing
 134 the weighted first-order Delaunay mosaic. We will see how this can be done in Section 3.2.

135 In $d \geq 3$ dimension, not all cells of $\text{Del}_k(A)$ are simplicial, even if the points in A are
 136 in general position. The cells carry important information, which for some applications
 137 is essential and cannot be easily recovered from a triangulation. This poses an additional
 138 challenge because most algorithms for computing convex hulls or weighted first-order Delaunay
 139 mosaics return a triangulated version of the correct mosaic. As explained in the following
 140 section, we address this issue by predicting the cells from their corresponding rhomboids.

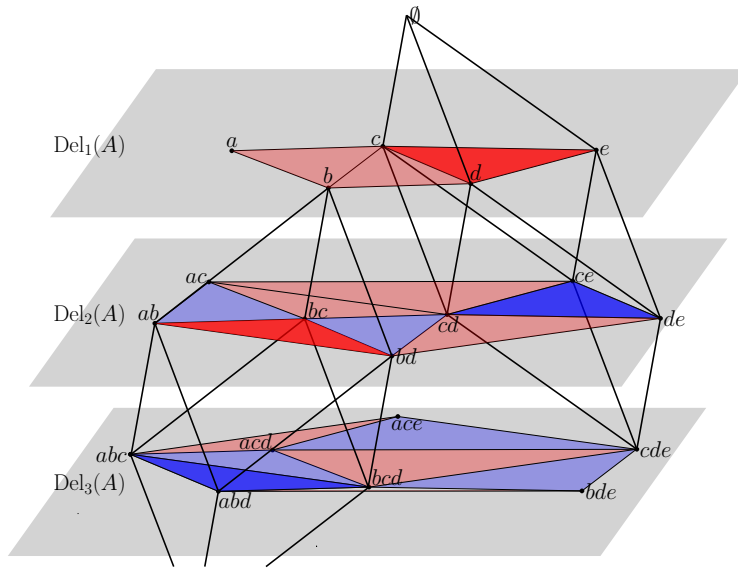
141 3.1 Predicting Cells

142 Given a cell σ in the order- k Delaunay mosaic, the following lemma identifies the rhomboid,
 143 ϱ , that σ is a slice of; see Figure 4 for an illustration. Write $V(\sigma)$ for the set of combinatorial
 144 vertices whose locations are the vertices of σ . Clearly, $V(\sigma) \subseteq V(\varrho)$.

145 ► **Lemma 2.** *Let $\varrho \in \text{Rho}(A)$ be a rhomboid and $\sigma \in \text{Del}_k(A)$ a slice of ϱ . Then $A_{in}(\varrho) =$
 146 $\bigcap V(\sigma)$, $A_{on}(\varrho) = \bigcup V(\sigma) \setminus A_{in}(\varrho)$, and the generation of σ is $k - \#A_{in}(\varrho)$.*

147 **Proof.** Recall that $V(\varrho) = \{A_{in}(\varrho) \subseteq Q \subseteq A_{in}(\varrho) \cup A_{on}(\varrho)\}$, in which $A_{in}(\varrho)$ and $A_{on}(\varrho)$
 148 are disjoint. Since the depth of a vertex is determined by its cardinality, and the vertices of
 149 a slice are by definition all at the same depth, the vertices of the generation- g slice all satisfy
 150 $\#Q - \#A_{in}(\varrho) = g$. The intersection of all g -subsets of $A_{on}(\varrho)$ is of course empty, which
 151 implies that the intersection of the combinatorial vertices of the slice is $A_{in}(\varrho)$. Furthermore,
 152 $\bigcup V(\sigma) = \bigcup V(\varrho)$ for every slice σ of ϱ with generation $g \geq 1$. The union of all g -subsets of
 153 $A_{on}(\varrho)$ is $A_{on}(\varrho)$ itself, and thus $A_{on}(\varrho) = \bigcup V(\sigma) \setminus A_{in}(\varrho)$. Finally, the generation of σ is
 154 the difference in depth of the anchor vertex, $A_{in}(\varrho)$, and the slice defining σ . The depth of σ
 155 is k and the depth of $A_{in}(\varrho)$ is its cardinality, which completes the proof. ◀

160 If all of our order- k Delaunay cells are triangulated—e.g. due to being the output of a
 161 weighted first-order Delaunay algorithm—we cannot directly apply Lemma 2. Indeed, if τ
 162 is a simplex that is part of a triangulation of a slice σ of a rhomboid ϱ , then $\bigcap V(\tau)$ and
 163 $\bigcup V(\tau)$ do not necessarily equal $A_{in}(\varrho)$ and $A_{in}(\varrho) \cup A_{on}(\varrho)$. We can, however, still identify



156 **Figure 4** First-, second-, and third-order Delaunay mosaics of the set $A = \{a, b, c, d, e\}$ in \mathbb{R}^2 as
 157 slices of the 3-dimensional rhomboid tiling. For clarity, only two of the rhomboids are shown, with
 158 their first-generation slices in red and second-generation slices in dark blue. The rhomboids on the
 159 left and right are defined by $A_{in} = \{b\}$, $A_{on} = \{a, c, d\}$ and $A_{in} = \emptyset$, $A_{on} = \{c, d, e\}$, respectively.

164 whether τ is a first-generation slice of ϱ and thus in fact is equal to σ . Using Lemma 2, we
 165 can then obtain ϱ .

166 **Lemma 3.** *A d -simplex, τ , in a triangulation of $\text{Del}_k(A)$ is a first-generation d -cell of*
 167 *$\text{Del}_k(A)$ if and only if the intersection of its combinatorial vertices is of size $k - 1$.*

168 **Proof.** Let σ be the d -cell in $\text{Del}_k(A)$ that contains τ in its triangulation, and assume σ is
 169 a generation- g slice of ϱ . From Lemma 2, we know that $A_{in}(\varrho) \subseteq v$ for all $v \in V(\sigma)$, and
 170 $\#A_{in}(\sigma) = k - g$. The remaining g points in every v are from $A_{on}(\varrho)$. We have $V(\tau) \subseteq V(\sigma)$
 171 with $\#V(\tau) = d + 1$. So for τ to consist of vertices whose common intersection is of size $k - 1$,
 172 there need to be $d + 1$ distinct g -subsets of $A_{on}(\varrho)$ that all have $g - 1$ points in common.
 173 However, as $\#A_{on}(\varrho) = d + 1$, this is not possible unless $g = 1$. \blacktriangleleft

174 3.2 Identifying Vertices

175 Given a triangulation of the order- k Delaunay mosaic, we just saw how to identify its
 176 first-generation cells. From these, we can obtain the corresponding rhomboids and their
 177 higher-generation slices. We shall now prove that if we have triangulations of the order- j
 178 Delaunay mosaics, for all $j < k$, we can assemble the complete vertex set of the order- k
 179 Delaunay mosaic by taking slices at depth k obtained from first-generation cells at lower
 180 depths. We note that this only holds in the unweighted setting.

181 To prepare the proof of this result, we recall the definition of the hyperplane arrangement
 182 postulated by Proposition 1. For each point $a \in A$, write $f_a: \mathbb{R}^d \rightarrow \mathbb{R}$ for the affine map
 183 defined by $f_a(x) = 2\langle x, a \rangle - \|a\|^2 = \|x\|^2 - \|x - a\|^2$. The graph of f_a is a hyperplane in
 184 \mathbb{R}^{d+1} that is tangent to the paraboloid \mathcal{P} of points $(x, z) \in \mathbb{R}^d \times \mathbb{R}$ that satisfy $z = \|x\|^2$.
 185 The collection of such hyperplanes decomposes \mathbb{R}^{d+1} into convex cells, which we call the
 186 *hyperplane arrangement* of A , denoted $\text{Arr}(A)$; see Figure 2. The *cells* in the arrangement

187 are intersections of hyperplanes and closed half-spaces. More formally, for each cell there
 188 is an ordered three-partition $A = A_{in} \sqcup A_{on} \sqcup A_{out}$ such that the cell consists of all points
 189 $(x, z) \in \mathbb{R}^d \times \mathbb{R}$ that satisfy $z \leq f_a(x)$, if $a \in A_{in}$; $z = f_a(x)$, if $a \in A_{on}$; and $z \geq f_a(x)$, if
 190 $a \in A_{out}$. This three-partition is the key to establishing the bijection between the cells of
 191 $\text{Arr}(A)$ and the rhomboids of $\text{Rho}(A)$ that proves the duality claimed in Proposition 1. We
 192 call top-dimensional cells of $\text{Arr}(A)$ *chambers*; they satisfy $A_{on} = \emptyset$. The depth of a chamber
 193 is $\#A_{in}$ or, equivalently, the number of hyperplanes that are above this chamber; it equals
 194 the depth of the dual vertex in $\text{Rho}(A)$. To see the aforementioned relationship between
 195 the arrangement and the higher-order Voronoi tessellations, we observe that the chamber in
 196 $\text{Arr}(A)$ with $A_{in} = Q$ vertically projects to $\text{dom}(Q)$. We can therefore construct $\text{Vor}_k(A)$ by
 197 computing and projecting all chambers whose ordered three-partitions satisfy $\#A_{in} = k$; see
 198 [8, Chapter 13] or [11].

199 We call a chamber γ a *bowl* if only one of its facets bounds it from above or, equivalently,
 200 if there is only one chamber at the next lower depth that shares a facet with γ . We call the
 201 hyperplane that contains this facet the *lid* of the bowl.

202 ► **Lemma 4.** *A hyperplane that is a lid of a bowl at depth 1 is not a lid of any other chambers.*

203 **Proof.** Let γ be a bowl at arbitrary depth, and let P be its lid. Every other hyperplane
 204 that contains a facet of γ bounds γ from below. The top facet of γ is the only part of P
 205 that is above all of these hyperplanes; that is: all other parts of P are below at least one of
 206 the other hyperplanes. This implies that every other bowl with lid P has at least one other
 207 hyperplane above it, and is thus of depth at least 2.

208 Now assume γ is at depth 1. If there were another bowl γ' with lid P , then the above
 209 argument would yield that all other bowls are at depth at least 2, contradicting our assumption
 210 on γ . Thus γ has to be the unique bowl with lid P . ◀

211 With this lemma, we are ready to state and prove the main combinatorial insight that
 212 motivates our algorithm. In a nutshell, it says that the first-generation cells form clusters
 213 without interior vertices. In \mathbb{R}^2 , this is equivalent to saying that these clusters have outer-
 214 planar 1-skeletons.

215 ► **Theorem 5.** *Let $A \subseteq \mathbb{R}^d$ be locally finite and $k \geq 2$. Then every vertex in $\text{Del}_k(A)$ is*
 216 *vertex of some d -cell of generation $g \geq 2$.*

217 **Proof.** In the unweighted setting, each hyperplane is tangent to the paraboloid \mathcal{P} and
 218 contains a facet of the unique depth-0 chamber. Thus, each hyperplane is the lid to a
 219 chamber at depth 1. As this is true for every hyperplane, all chambers of depth 2 or higher
 220 have no lids by Lemma 4. This means that any chamber of depth at least 2 has at least two
 221 upper facets. Because the upper boundary is connected, there are two upper facets that
 222 meet in a $(d - 1)$ -face, the dual rhomboid of this face has dimension 2, and its bottom vertex
 223 is dual to the chamber. Thus we can obtain this vertex, v , knowing the other three vertices
 224 of the 2-rhomboid.

225 Any 2-rhomboid is a face of some $(d + 1)$ -dimensional rhomboid, ϱ , which thus contains v
 226 at generation at least 2, i.e. v has depth at least $\#A_{in}(\varrho) + 2$. Knowing $A_{in}(\varrho)$ and $A_{on}(\varrho)$,
 227 we obtain this vertex via Equation (1). ◀

228 4 Algorithm

229 We outline our algorithm in this section; its correctness follows from the results of the
 230 previous sections. We compute the Delaunay mosaics one by one in sequence of increasing

231 order. For $\text{Del}_1(A)$, the vertex set is the set A of input points. Whenever we have the vertex
 232 set of $\text{Del}_j(A)$, we compute its (triangulated) d -cells using an off-the-shelf algorithm for
 233 weighted Delaunay triangulations. We use Lemma 3 to identify the first-generation d -cells,
 234 while discarding all other cells. From each first-generation cell, we obtain and save the
 235 higher-generation d -cells and vertices defined by the same rhomboid. These will appear in
 236 Delaunay mosaics of higher orders. By Theorem 5, once we have processed all $\text{Del}_j(A)$ for
 237 $j < k$, we will have obtained the complete vertex set of $\text{Del}_k(A)$ in the process, thus allowing
 238 our algorithm to continue until we have all Delaunay mosaics up to the desired order.

239 Algorithm 1 is a more formal write-up of the above outline, and Figure 4 visualizes
 240 the process. A dimension-agnostic `python` implementation and a 2- and 3-dimensional `C++`
 241 implementation using CGAL [22] are available at [19, 20]. If we store all first-generation cells
 242 with their anchor vertices, we can use this algorithm to implicitly construct the rhomboid
 243 tiling, as done in [20].

240 To get a handle on the runtime of the algorithm, we consider the two steps used to
 241 compute the order- k Delaunay mosaic after finishing the construction of the first $k - 1$ mosaics.
 242 The first step is geometric and invokes the black-box algorithm to construct the weighted
 243 Delaunay mosaic from which we get vertices and cells of (unweighted) higher-order Delaunay
 244 mosaics. The runtime of this step depends on the runtime of the black box algorithm, which
 245 in many cases is output-dependent. The second step is combinatorial and determines, for each
 246 output simplex from the first step, whether it is first generation, in which case it is a genuine
 247 cell of the mosaic. Assuming constant dimension, d , identifying whether an order- $(k - 1)$ cell
 248 is of first generation and, in this case, obtaining the higher-generation cells takes time $O(k)$.
 249 Thus, for a given k , the combinatorial step takes time $O(kC_k)$, in which C_k is the number of
 250 d -cells of $\text{Del}_k(A)$. With each vertex being represented as a k -tuple of points, this is linear
 251 in the output size, assuming we store each cell naively as a set of its vertices. If the runtime
 252 of each black-box invocation were linear in the output size, the total runtime for producing
 253 the first k higher-order Delaunay mosaics would thus be linear in the output size as well.

254 In practice, it is more efficient to store a cell as a set of pointers or indices to its vertices,
 255 only requiring space $O(kV_k + C_k)$, with V_k denoting the number of vertices of $\text{Del}_k(A)$. Using
 256 this representation, the combinatorial step is not linear in the output size unless the number
 257 of cells of $\text{Del}_k(A)$ is linear in the number of vertices.

258 5 Experimental Results

259 In 2 dimensions, the number of cells in the (order-1) Delaunay mosaic is always linear in the
 260 number of input points, while in $d \geq 3$ dimensions, the size of the mosaic depends on the
 261 input set itself—and not just its cardinality—and ranges from $\Omega(n)$ to $O(n^{\lceil d/2 \rceil})$ [16]. The
 262 asymptotic worst case is realized by points located on the moment curve, (t, t^2, \dots, t^d) with
 263 $t \in \mathbb{R}$, while e.g. uniformly sampled points within a sphere have expected linear size [7], as
 264 do uniformly sampled points on a convex polytope in \mathbb{R}^3 [12]. Under appropriate sampling
 265 conditions for points on a smooth surface, the size of the mosaic is $O(n \log n)$ [3].

268 *Size in 3 dimensions.* To shed light on the size range of order- k Delaunay mosaics, we
 269 compute them for a few 3-dimensional point sets relevant to these bounds. Note that for
 270 order- k Delaunay mosaics the number of vertices varies as well. Figure 5 shows the numbers
 271 of vertices and 3-dimensional cells for all higher-order Delaunay mosaics of four sets of size
 272 $n = 200$ each: points on the `moment curve`, points sampled on the `torus` (with major radius
 273 1 and minor radius 0.5 obtained by uniformly sampling the angles of its parametrization),
 274 points uniformly sampled inside the `unit ball`, and a point set in convex position forming

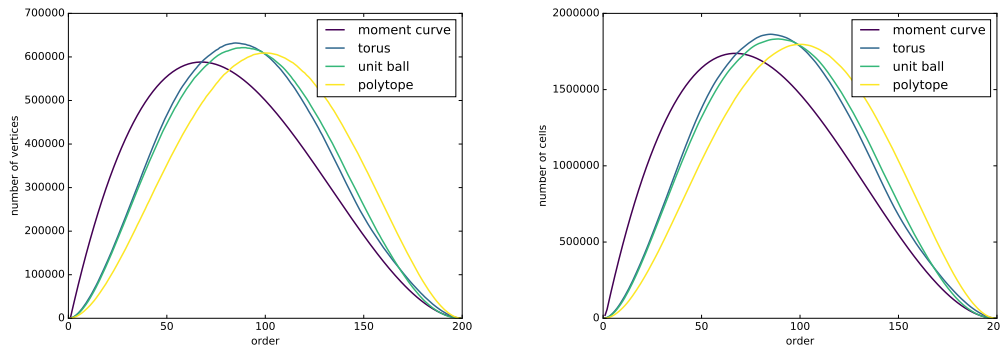
244 **Algorithm 1** computes the order- k Delaunay mosaic of a finite set of (unweighted) points,
 245 $A \subseteq \mathbb{R}^d$. We represent each d -cell of $\text{Del}_k(A)$ by the collection of its combinatorial vertices,
 246 stressing that these collections are sets and thus contain every combinatorial vertex only
 247 once. Duplicity is avoided by checking before adding. The locations of the combinatorial
 248 vertices are the barycenters of their points, and the cell is the convex hull of these locations.
 249 While the software for computing the weighted Delaunay mosaic may return all cells triangulated,
 250 our algorithm outputs the (non-triangulated) cells of the order- k Delaunay mosaic.
 251 We recall that in $d \geq 3$ dimensions such non-simplicial cells appear generically for $k \geq 2$.

```

252  $V(\text{Del}_1(A)) := A$ 
253 for  $j$  from 1 to  $k$  do
254   // Compute the location and weight of each combinatorial vertex
255   for all  $v \in V(\text{Del}_j(A))$  do
256      $loc(v) := \frac{1}{j} \sum_{a \in v} a$ 
257      $wt(v) := \|\frac{1}{j} \sum_{a \in v} a\|^2 - \frac{1}{j} \sum_{a \in v} \|a\|^2$ 
258   end for
259   // Get the (triangulated) cells of the order- $j$  Delaunay mosaic
260    $D := \text{weightedDelaunay}(loc, wt)$ 
261   // Infer vertices and higher-generation cells of later Delaunay mosaics
262   for all  $d$ -simplices  $\sigma$  in  $D$  do
263     // Check whether the generation of  $\sigma$  is 1 via Lemma 3
264     // We already obtained higher-generation cells of  $\text{Del}_j(A)$  earlier.
265     if  $\#\cap V(\sigma) = j - 1$  then
266       Add  $\sigma$  to  $\text{Del}_j(A)$ 
267       // Get  $A_{in}(\varrho)$  and  $A_{on}(\varrho)$  via Lemma 2
268        $A_{in}(\varrho) := \cap V(\sigma)$ 
269        $A_{on}(\varrho) := \cup V(\sigma) \setminus A_{in}(\varrho)$ 
270       for  $g$  from 2 to  $d$  do
271         // Get the generation- $g$  cell,  $\sigma'$ , of the rhomboid of  $\sigma$ , via Equation (1)
272          $V(\sigma') := \{A_{in}(\varrho) \cup Q \mid Q \in A_{on}(\varrho), \#Q = g\}$ 
273         Add all  $v \in V(\sigma')$  to  $V(\text{Del}_{j+g-1}(A))$ 
274         Add  $\sigma'$  to  $\text{Del}_{j+g-1}(A)$ 
275       end for
276     end if
277   end for
278 end for
279 return  $V(\text{Del}_k(A)), \text{Del}_k(A)$ 

```

315 a **polytope** (obtained by uniformly sampling points inside a ball and randomly choosing 200
 316 vertices of the convex hull). The plots of vertex numbers and cell numbers generally resemble



306 ■ **Figure 5** Number of vertices (*left*) and of 3-dimensional cells (*right*) in the order- k Delaunay
 307 mosaics of four sets with $n = 200$ points in \mathbb{R}^3 each.

316
 317 each other, with roughly three times as many cells as vertices. Other than in Figure 5, we
 318 therefore omit the information about the vertices and show only the plots for the cells. The
 319 **moment curve** and **polytope** sets are both in convex position. Nevertheless, the size of the
 320 mosaic for the **moment curve** grows large faster for small k , and reaches its peak at $k \approx n/3$,
 321 while for the **polytope** the peak is at $k \approx n/2$. Notice how a faster rise also goes along with
 322 an earlier decay. This is a consequence of the fact that the total size of all order- k Delaunay
 323 mosaics together—or, equivalently of the rhomboid tiling—only depends on the input size, n ,
 324 and not on the relative position of the input points.

325 *Size increase for small order.* Looking more closely at the growth for small k relative to the
 326 input size, we observe that the **polytope** and **unit ball** exhibit linear growth while the
 327 size of the mosaic seems to grow quadratically for the **moment curve**, see Figure 6. This is
 328 consistent with the bounds on first-order Delaunay mosaics mentioned earlier. For the **torus**,
 329 the size seems to grow slightly superlinearly, which is again consistent with the $O(n \log n)$
 330 bound for smooth surfaces mentioned above.

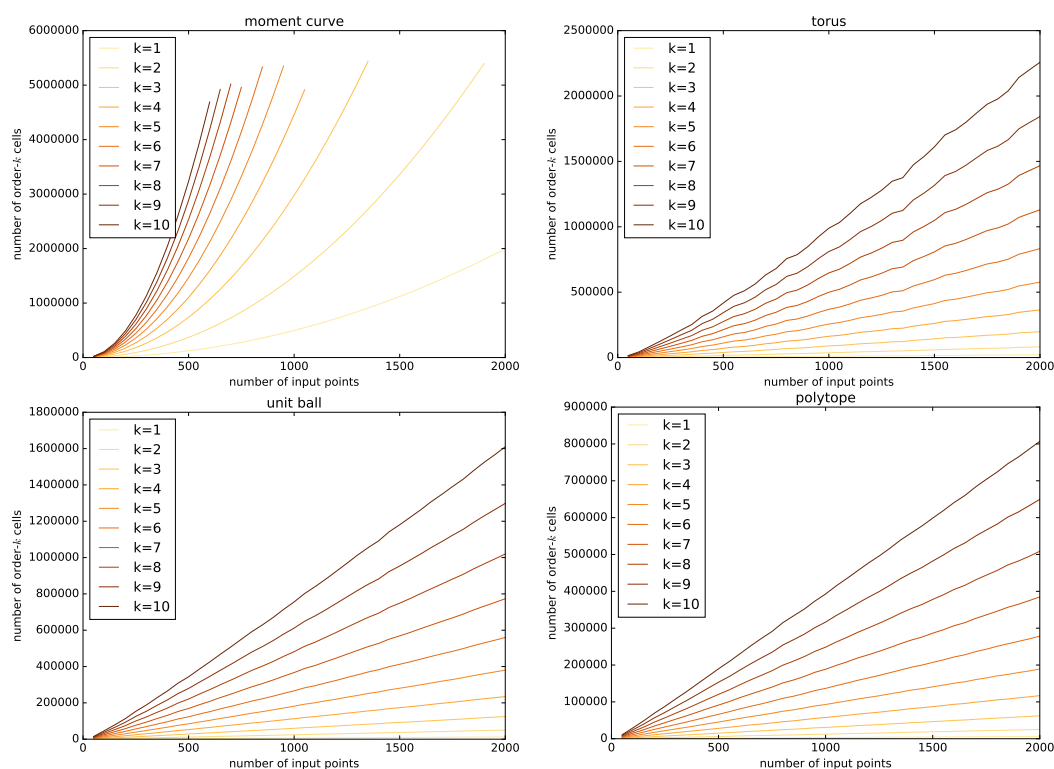
337 *Variance.* To probe whether the above figures are representative, we investigate the variance
 338 in number of cells for the **polytope** and the **unit ball**. As shown in Figure 7, the variance is
 339 particularly small for the **polytope**, and it is considerably larger of the **unit ball**. Curiously,
 340 the variance dips at $k = n/2$.

343 *Generations.* We also investigate the distribution of cells of different generations. All point
 344 sets exhibit a pattern similar to that in Figure 8, with the fraction of first-generation cells
 345 decreasing and the fraction of d -th-generation cells increasing as the order grows. The change
 346 is most prominent for small and large k , while the fractions remain almost constant in the
 347 range $k \approx n/2$, provided n is significantly larger than the dimension d .

350 *Curse of dimensionality.* Like many geometric structures, order- k Delaunay mosaics are
 351 subject to the dimensionality curse. Figure 9 shows how the size of order- k Delaunay mosaics
 352 behaves for point sets in different dimensions.

355 *Vertex degrees.* Order- k Delaunay mosaics in \mathbb{R}^3 exhibit an interesting distribution of vertex
 356 degrees for random point sets; see Figure 10. The distribution looks like the sum of two
 357 distributions—with the second one only covering values 2 modulo 3—and is exhibited for

XX:10 A Simple Algorithm for Higher-order Delaunay Mosaics and Alpha Shapes



331 ■ **Figure 6** Number of cells in the order- k Delaunay mosaics for small k in relation to the input
332 size, for various 3-dimensional point sets.

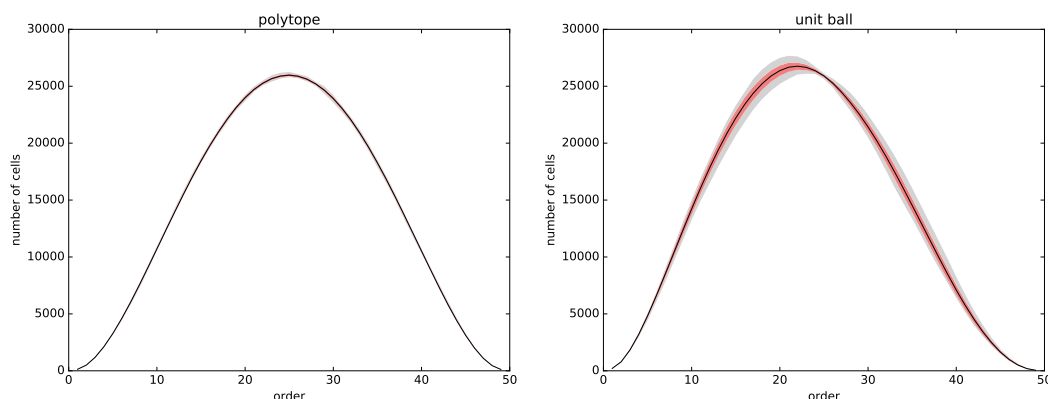
358 all k except very small and very large ones. We do not know the reason for vertices being
359 frequently incident to 5, 8, 11, \dots d -cells, but suspect these numbers correspond to geometric
360 configurations of cells of different generations, such as three octahedra sharing a common
361 vertex with two tetrahedra.

364 *Clusters.* First-generation cells of any order- k Delaunay mosaic come in clusters connected
365 by shared facets. We investigate the distribution of their sizes, leaving the discussion of
366 their potential algorithmic significance for later. Figure 11 shows cluster size distributions in
367 \mathbb{R}^3 for different orders. For very small k , the distribution depends on how the points are
368 sampled, while for all other k , the cluster sizes seem to follow an exponential distribution.
369 The decay rate increases with k and seems to be linked to the fraction of first-generation
370 cells. It culminates in all clusters being singletons for $k = n - 3$. For $k > n - 3$, there are no
371 more first-generation cells.

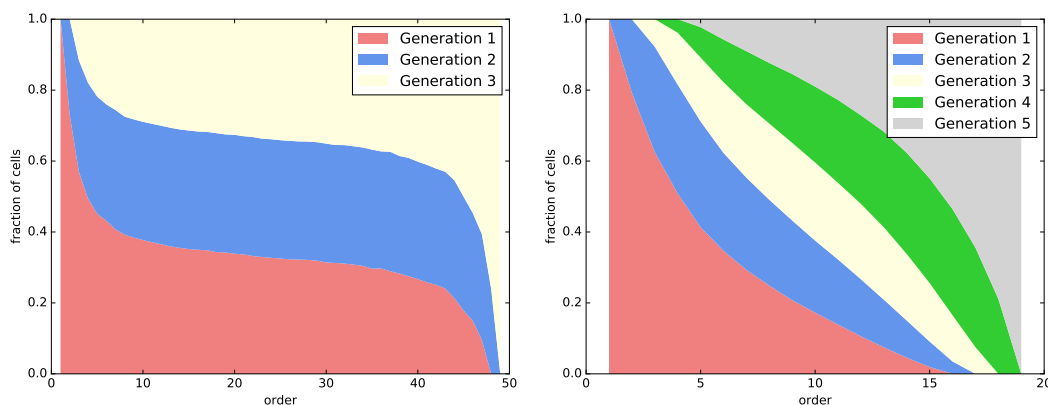
372 **6** Order- k Alpha Shapes

373 Beyond order- k Delaunay mosaics, our algorithm can be extended to compute *order- k alpha*
374 *shapes*, as introduced in [14]. To this end, the rhomboid tiling is endowed with a radius
375 function on its rhomboids [10]. It is inherited by the Delaunay mosaics, which are slices of
376 the rhomboid tiling, and their sublevel sets with respect to this radius function are complexes
377 that geometrically realize the order- k α -shapes. In this section, we recall the definition of
378 the radius function from [10], and present an efficient way of computing it.

379 To get started, we note that the radius function needs a representation for every rhomboid



333 **Figure 7** Variance of the number of 3-dimensional cells in the order- k Delaunay mosaics of
 334 randomly sampled points in convex position (*left*) and in a unit ball (*right*). The statistics of each
 335 plot are obtained from 30 sets of 50 points each. In *black*: the mean; in *red*: the range of one
 336 standard deviation around the mean; in *grey*: the range between the minimum and maximum.



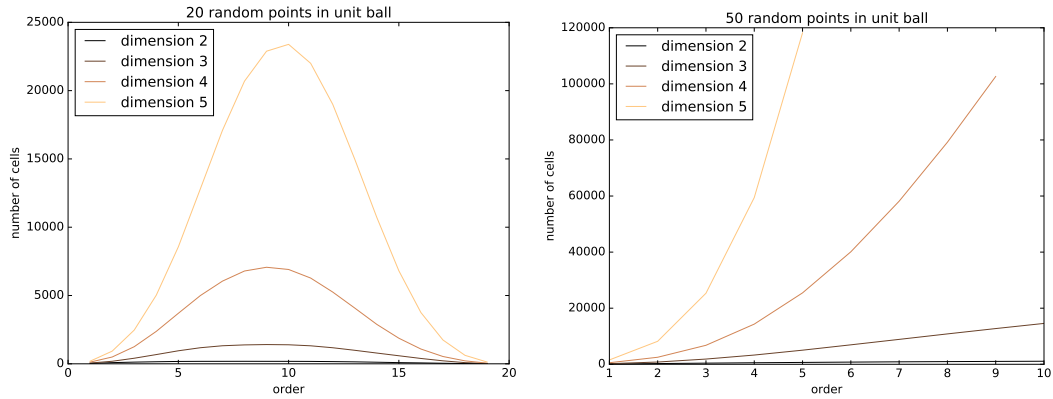
341 **Figure 8** Fraction of cells of each generation in the order- k Delaunay mosaic, for 50 random
 342 points in the unit 3-ball (*left*) and 20 random points in the unit 5-ball (*right*).

380 in the tiling, but the algorithm in Section 4 computes only the top-dimensional rhomboids.
 381 This is easily remedied by noticing that the dimension of a rhomboid is $k = \#A_{on}(\varrho)$ and
 382 its 3^k faces correspond to the different ways of partitioning $A_{on}(\varrho)$ into three sets. For the
 383 remainder of the discussion, assume that we have a representation for the rhomboids of all
 384 dimensions $0 \leq j \leq d+1$ in $\text{Rho}(A)$. Each j -dimensional rhomboid, $\varrho \in \text{Rho}(A)$, corresponds
 385 to a $(d+1-j)$ -dimensional cell in the dual arrangement, $\varrho^* \in \text{Arr}(A)$. We introduce
 386 $\mathcal{P}_t(x): \mathbb{R}^d \rightarrow \mathbb{R}$ defined by mapping $x \in \mathbb{R}^d$ to $\mathcal{P}_t(x) = \frac{1}{2}(\|x\|^2 - t)$. With slight abuse of
 387 notation, we write \mathcal{P}_t for the graph of this function. This graph is the paraboloid \mathcal{P}_0 dropped
 388 down vertically by a distance $\frac{t}{2}$. We define the *squared radius function* $\mathcal{R}^2: \text{Rho}(A) \rightarrow \mathbb{R}$,
 389 which maps a rhomboid to the minimum t such that \mathcal{P}_t has a non-empty intersection with ϱ^* .
 390 We call a sphere *constrained* by ϱ if it encloses $A_{in}(\varrho)$, passes through all points of $A_{on}(\varrho)$,
 391 and has no other points of A inside. Letting $S_{min}(\varrho)$ be the smallest such sphere, we get an
 392 alternative interpretation of the radius function:

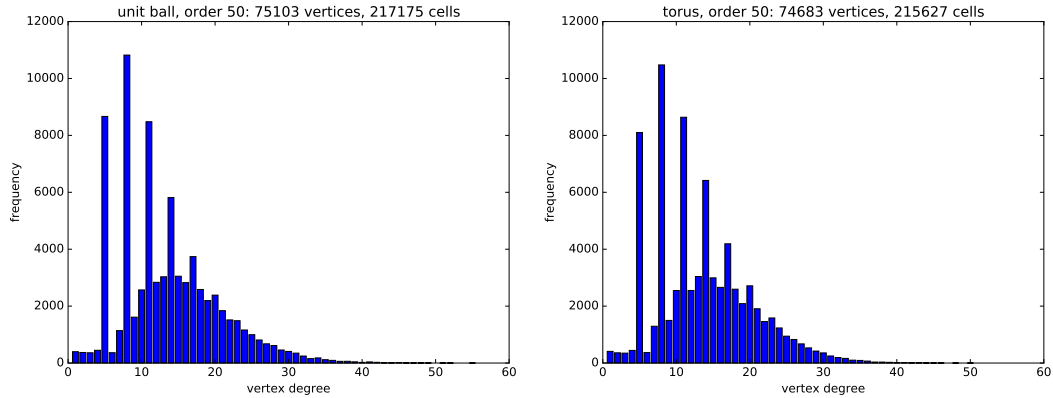
393 **► Lemma 6.** $\mathcal{R}^2(\varrho)$ equals the squared radius of $S_{min}(\varrho)$.

394 **Proof.** The proof of Theorem 1 of [10] establishes a map from points in the $\text{Arr}(A)$ to spheres:

XX:12 A Simple Algorithm for Higher-order Delaunay Mosaics and Alpha Shapes



348 **Figure 9** Number of d -cells in the order- k Delaunay mosaic for 20 points (*left*) and 50 points
 349 (*right*) randomly sampled in the unit ball for different dimensions d .

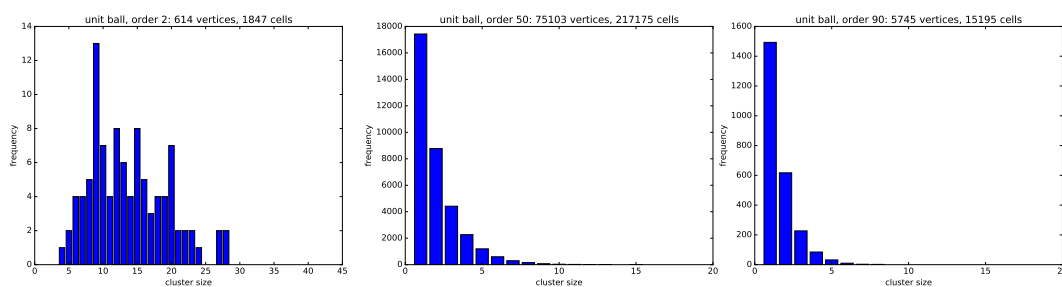


353 **Figure 10** Vertex degree distribution in the order-50 Delaunay mosaic for 100 points sampled in
 354 the unit ball (*left*) and on the torus (*right*).

395 a point $y = (x, z) \in \mathbb{R}^d \times \mathbb{R}$ below the paraboloid \mathcal{P} is mapped to the sphere, S , with center
 396 x and squared radius $\|x\|^2 - 2z$. Importantly, if ϱ^* is the cell in the dual arrangement whose
 397 interior contains y , then S is constrained by ϱ , which is the rhomboid dual to ϱ^* .

398 Now let $t = \mathcal{R}^2(\varrho)$, and let r^2 be the squared radius of $S_{\min}(\varrho)$. By definition, t is the
 399 smallest value for which \mathcal{P}_t contains a point $y \in \varrho^*$. The aforementioned map maps y to
 400 a sphere constrained by ϱ , thus $r^2 \leq t$. When reversing this map, $S_{\min}(\varrho)$ is mapped to a
 401 point of ϱ^* . As t was the smallest value for which \mathcal{P}_t touches ϱ^* , we have $t \leq r^2$. Thus the
 402 squared radius of $S_{\min}(\varrho)$ equals $\mathcal{R}^2(\varrho)$. \blacktriangleleft

403 To compute this radius function, we first get the smallest sphere constrained by a
 404 rhomboid. While Welzl's algorithm [23] for smallest enclosing sphere can be adapted to this
 405 task, it takes $O(n)$ with $n = \#A$ for each such sphere computation. To improve on this
 406 bound, we recall that Lemma 3 of [10] establishes that rhomboids of the same radius value
 407 come in intervals $[\varrho_{\min}, \varrho_{\max}] := \{\varrho \in \text{Rho}(A) \mid \varrho_{\min} \subseteq \varrho \subseteq \varrho_{\max}\}$ whose lower bound, ϱ_{\min} ,
 408 is a vertex. To identify the vertex v that a rhomboid ϱ forms an interval with, we need to
 409 identify its vertex with the same radius value. By Lemma 6 this means the radii of $S_{\min}(\varrho)$
 410 and $S_{\min}(v)$ have to be the same, and it is not difficult to see that the spheres $S_{\min}(\varrho)$ and
 411 $S_{\min}(v)$ are in fact the same. As $A_{\text{on}}(v) = \emptyset$ for any vertex v , the sphere achieving the radius
 412 value of v is defined solely by inclusions and exclusion constraints. Therefore all constraints



362 **Figure 11** From *left to right*: distribution of cluster sizes in Delaunay mosaics of order 2, 50, and
 363 90 for 100 random points in the **unit ball**.

413 of ϱ that require points of $A_{on}(\varrho)$ to be on the sphere need to be converted to inclusion and
 414 exclusion constraints without affecting the resulting sphere. We know that such constraints
 415 exist because the lower bound of the interval is a vertex. This observation gives rise to the
 416 following lemma.

417 **► Lemma 7.** *Let ϱ be a rhomboid that is an upper bound of an interval. Let $A_I \subseteq A_{on}(\varrho)$
 418 such that the smallest enclosing sphere S of A_I that excludes $A_{on}(\varrho) \setminus A_I$ is the same as the
 419 circumsphere of $A_{on}(\varrho)$. Then ϱ forms an interval with the vertex $v = A_{in}(\varrho) \cup A_I$.*

420 **Proof.** As ϱ is an upper bound of an interval, its sphere, $S_{min}(\varrho)$, is only supported by
 421 $A_{on}(\varrho)$. Indeed, if there were another point $a \in A_{in}(\varrho)$ —or $a \in A_{out}(\varrho)$ —on the surface of
 422 this sphere, then the rhomboid ϱ with $A_{on}(\varrho) = A_{on}(\varrho) \cup \{a\}$ and $A_{in}(\varrho) = A_{in}(\varrho) \setminus \{a\}$ —or
 423 $A_{out}(\varrho) = A_{out}(\varrho) \setminus \{a\}$ —would be a higher-dimensional rhomboid with the same sphere
 424 $S_{min}(\varrho) = S_{min}(\varrho)$, contradicting that ϱ be an upper bound of an interval.

425 As $S_{min}(\varrho)$ is only supported by $A_{on}(\varrho)$, this means that $S_{min}(\varrho)$ is the same as the
 426 circumsphere of $A_{on}(\varrho)$, which by our assumption is the same as S . Now the inclusion and
 427 exclusion constraints of S are part of the constraint set for $S_{min}(v)$, but because $S = S_{min}(\varrho)$
 428 it does in fact fulfill all the constraints of $S_{min}(v)$. Thus $S_{min}(v) = S = S_{min}(\varrho)$, proving
 429 that they are in the same interval. ◀

430 **Algorithm.** Assume ϱ is a j -rhomboid that is an upper bound of an interval. Let S be the
 431 circumsphere of $A_{on}(\varrho)$. For each point $a \in A_{on}(\varrho)$, we need to decide whether to impose
 432 an inclusion or exclusion constraint on it. Let S_a be the circumsphere of $A_{on}(\varrho) \setminus \{a\}$. If a
 433 is outside of S_a , then imposing an exclusion constraint for a would yield S_a rather than S ,
 434 thus we add a to A_I in order to impose an inclusion constraint for it. Similarly, if a is inside
 435 of S_a , we have to impose an exclusion constraint for a and thus do not add it to A_I .

436 While this is difficult for an individual rhomboid, it becomes straightforward if we compute
 437 all intervals in the rhomboid tiling. We know that all $(d+1)$ -rhomboids are upper bounds of
 438 intervals. After marking all rhomboids that are contained in such intervals, we know that
 439 all remaining unmarked d -rhomboids are upper bounds of intervals. Thus by processing the
 440 rhomboids in decreasing dimension, all unmarked rhomboids we encounter are upper bounds.

441 **7 Discussion**

442 This paper presents a simple algorithm for computing order- k Delaunay mosaics in Euclidean
 443 space of constant dimension. Implementations of the algorithm—in **C++** for points in \mathbb{R}^2
 444 and \mathbb{R}^3 and in **python** for points in \mathbb{R}^d —are provided [19, 20]. This software includes the

445 application to the persistence of k -fold covers described in [10]. The remainder of this section
 446 discusses this application and possible extensions and optimizations of our algorithm.

447 *k -fold covers.* The sublevel sets of the order- k Delaunay mosaics with respect to the radius
 448 function introduced in Section 6 are homotopy equivalent to k -fold covers of Euclidean balls.
 449 It follows that our algorithms facilitate the computation of persistence of these k -fold covers.
 450 Furthermore, the circumcenters of the spheres that are used in the computation of the
 451 radius function provide the geometric locations of the order- k Voronoi vertices and allow
 452 reconstructing the order- k Voronoi tessellation via duality.

453 *Weighted setting.* Our algorithm generalizes to points with real weights, but not easily. The
 454 main challenge is the extraction of the vertices of the order- k mosaic from lower-order mosaics.
 455 This extraction relies on Theorem 5, which does not hold for weighted points. Indeed, a
 456 crucial assumption in this theorem is that every lifted hyperplane is incident to the depth-0
 457 chamber of the arrangement, and this property is generally violated for weighted points. This
 458 is the same assumption used in the prior dimension-agnostic algorithms [1, 17, 18]. For sets
 459 of weighted points that satisfy this assumption, our algorithm and these prior algorithms
 460 still work. To overcome this limitation, we would need a way to detect all bowls in the
 461 arrangement, because they correspond to the vertices in the Delaunay mosaics our algorithm
 462 is not able to find. Identifying the bowls is an independent problem, and any solution to it
 463 can be combined with our algorithm. Once we know the bowls and add the corresponding
 464 vertices to the appropriate mosaics, our algorithm works as before.

465 *Clusters of cells.* As mentioned in Section 5, first-generation cells in the order- k Delaunay
 466 mosaic are organized in clusters. To formally define them, consider the graph whose nodes
 467 are the cells and whose arcs are the shared facets (i.e. the 1-skeleton of the order- k Voronoi
 468 tessellation). A *cluster* is a connected component in the subgraph induced by the first-
 469 generation cells. It is not difficult to see that two such cells belong to a common cluster if
 470 and only if the corresponding rhomboids have the same anchor vertex. Let ϱ be one of these
 471 rhomboids and recall that the anchor vertex is $A_{in}(\varrho)$, which in this case is a collection of
 472 $k - 1$ points of A . Each combinatorial vertex of any cell in the cluster contains these $k - 1$
 473 points, plus one additional point, which differentiates between these vertices. In other words,
 474 the cluster as a subcomplex of the order-1 Delaunay mosaic of these additional points.

475 With this insight, we could replace the weighted Delaunay mosaic of the entire vertex
 476 set by multiple instances of unweighted Delaunay mosaics, namely one per cluster. This
 477 alternative strategy avoids the need to compute averages of points at the cost of extra
 478 book-keeping to group the vertex set of $\text{Del}_k(A)$ into clusters. We mention that in \mathbb{R}^2 , the
 479 structure of each cluster satisfies the requirements that allow for the construction in time
 480 linear in the number of points [2].

481 *Exact arithmetic.* The CGAL software library [22] supports exact arithmetic by distinguishing
 482 between *exact constructions* and *exact predicates*. The latter are geometric tests with a **true**
 483 or **false** answer, such as whether or not a given point lies on a given sphere. By itself, the
 484 CGAL algorithm for weighted Delaunay triangulations requires exact predicates but no exact
 485 constructions. Our algorithm, on the other hand, computes averages of collections of input
 486 points, which are the locations of the vertices of the mosaic. This is an exact construction
 487 and indeed the only one needed to run our algorithm with exact arithmetic. In practice,
 488 exact constructions are a significant overhead with noticeable impact on the runtime, which
 489 would be nice to avoid.

References

- 490 ——— **References** ———
- 491 **1** P.K. Agarwal, M. De Berg, J. Matousek, and O. Schwarzkopf. Constructing levels in arrange-
492 ments and higher order Voronoi diagrams. *SIAM J. Comput.*, 27(3):654–667, 1998.
- 493 **2** A. Aggarwal, L.J. Guibas, J. Saxe, and P.W. Shor. A linear-time algorithm for computing the
494 Voronoi diagram of a convex polygon. *Discrete Comput. Geom.*, 4:591–604, 1989.
- 495 **3** D. Attali, J.-D. Boissonnat, and A. Lieutier. Complexity of the Delaunay triangulation of
496 points on surfaces the smooth case. In *Proc. 19th Ann. Symp. Comput. Geom.*, pages 201–210,
497 2003.
- 498 **4** F. Aurenhammer. A new duality result concerning Voronoi diagrams. *Discrete Comput.*
499 *Geom.*, 5:243–254, 1990.
- 500 **5** F. Chazal, D. Cohen-Steiner, and Q. Mérigot. Geometric inference for probability measures.
501 *Found. Comput. Math.*, 11(6):733–751, 2011.
- 502 **6** K.L. Clarkson and P.W. Shor. Applications of random sampling in computational geometry,
503 II. *Discrete Comput. Geom.*, 4(1):387–421, 1989.
- 504 **7** R.A. Dwyer. Higher-dimensional Voronoi diagrams in linear expected time. *Discrete Comput.*
505 *Geom.*, 6(3):343–367, 1991.
- 506 **8** H. Edelsbrunner. *Algorithms in Combinatorial Geometry*. Springer-Verlag, Heidelberg,
507 Germany, 1987.
- 508 **9** H. Edelsbrunner, D. Kirkpatrick, and R. Seidel. On the shape of a set of points in the plane.
509 *IEEE Trans. Inform. Th.*, 29(4):551–559, 1983.
- 510 **10** H. Edelsbrunner and G. Osang. The multi-cover persistence of Euclidean balls. In *Proc. 34th*
511 *Ann. Symp. Comput. Geom.*, pages 34:1–34:14, 2018.
- 512 **11** H. Edelsbrunner and R. Seidel. Voronoi diagrams and arrangements. *Discrete Comput. Geom.*,
513 1(1):25–44, 1986.
- 514 **12** M.J. Golin and H.-S. Na. On the average complexity of 3d-Voronoi diagrams of random points
515 on convex polytopes. *Comput. Geom.*, 25(3):197–231, 2003.
- 516 **13** L.J. Guibas, D. Morozov, and Q. Mérigot. Witnessed k -distance. *Discrete Comput. Geom.*,
517 49(1):22–45, 2013.
- 518 **14** D. Krasnoshchekov and V. Polishchuk. Order- k α -hulls and α -shapes. *Inform. Process. Lett.*,
519 114(1-2):76–83, 2014.
- 520 **15** D.-T. Lee. On k -nearest neighbor Voronoi diagrams in the plane. *IEEE Trans. Comput.*,
521 31(6):478–487, 1982.
- 522 **16** P. McMullen. The maximum numbers of faces of a convex polytope. *Mathematika*, 17(2):179–
523 184, 1970.
- 524 **17** K. Mulmuley. Output sensitive construction of levels and Voronoi diagrams in \mathbb{R}^d of order 1
525 to k . In *Proc. 22nd Ann. ACM Symp. Theory Comput.*, pages 322–330, 1990.
- 526 **18** K. Mulmuley. On levels in arrangements and Voronoi diagrams. *Discrete Comput. Geom.*,
527 6(3):307–338, 1991.
- 528 **19** G. Osang. Higher order Delaunay mosaics in C++ and python. [https://github.com/geoo89/
529 orderkdelaunay](https://github.com/geoo89/orderkdelaunay), 2019.
- 530 **20** G. Osang. Rhomboid tiling and order- k Delaunay mosaics in C++. [https://github.com/
531 geoo89/rhomboidtiling](https://github.com/geoo89/rhomboidtiling), 2020.
- 532 **21** M.I. Shamos and D. Hoey. Closest-point problems. In *Proc. 16th Ann. IEEE Symp. Found.*
533 *Comput. Sci.*, pages 151–162, 1975.
- 534 **22** The CGAL Project. *CGAL User and Reference Manual*. CGAL Editorial Board, 5.0 edition,
535 2019. URL: <https://doc.cgal.org/5.0/Manual/packages.html>.
- 536 **23** E. Welzl. Smallest enclosing disks (balls and ellipsoids). In H.A. Maurer, editor, *Results and*
537 *New Trends in Computer Science*, pages 359–370. Springer-Verlag, 1991.